Chapter 6:

CRUSTAL STRUCTURE OF NW HIMALAYA

Chapter 6:

Seismological and Geophysical constraint to the crustal structure beneath the North Western Himalaya, India

6.1. Introduction

This chapter discusses the entire seismological and Geophysical study carried out in the NW Himalaya with a major tectonic implication obtained from various studies. This clearly shows the fact that the current seismotectonic scenario prevailing in the region is near to failure in future and major earthquakes are likely to occur. The estimated seismic potential for the region considering all the microseismicity in the region shows that only a fraction of energy (3–5 %) that has accommodated in the region due to under thrusting has been dissipated through occurrences of Great earthquakes and the remaining (95–97 %) can give rise to number of devastating earthquakes in future and cause a great loss to the socio-economic condition of the country.

6.2. 1 D Crustal velocity model and seismicity relocation using JHD

The seismic events recorded through the local network were used to derive the velocity structure of the region by travel-time inversion of P and S-waves, respectively. Due to shallow seismic activity in the region, the arrival times could only calculate the upper crustal velocity up to 30 km with more precision. This further gives the inference that the first discontinuity in this region lies at 18 km depth. So, this crustal part of the Himalaya is quite thicker as compared to other Himalaya parts. According to earlier studies by Hazarika et al. (2013) and our study, it is suggested that the Moho depth in this part of the Himalaya lies approximately between 50 and 60 km. The Vp/Vs ratio inferred from Wadati's plot gives a value of 1.74 with a standard deviation of 0.03s which is globally supported by earlier published results (Kumar et al.,

2009; Mukhopadhyay and Sharma 2010; Monsalve et al., 2008). While putting cross section across the known thrust faults namely MBT, MCT and STD, it is observed that the seismicity at MCT is mostly controlled by seismic activity taking place along these thrust faults and the maximum depth of the seismic events are restricted up to 30 km depth. Towards the north of MCT, the depth of the seismic events increases with effect of both MCT and STD faults. The seismic activity across the STD fault is high that is mainly controlled by the India-Eurasia collision. The cross section across the major thrust faults also coincide with the Kaurik-Chango Fault (KCF) - a normal fault having an N–S dip. The maximum seismicity lays both sides of the STD across the Kaurik fault which is responsible for the neotectonic activity (Joshi et al., 2010).

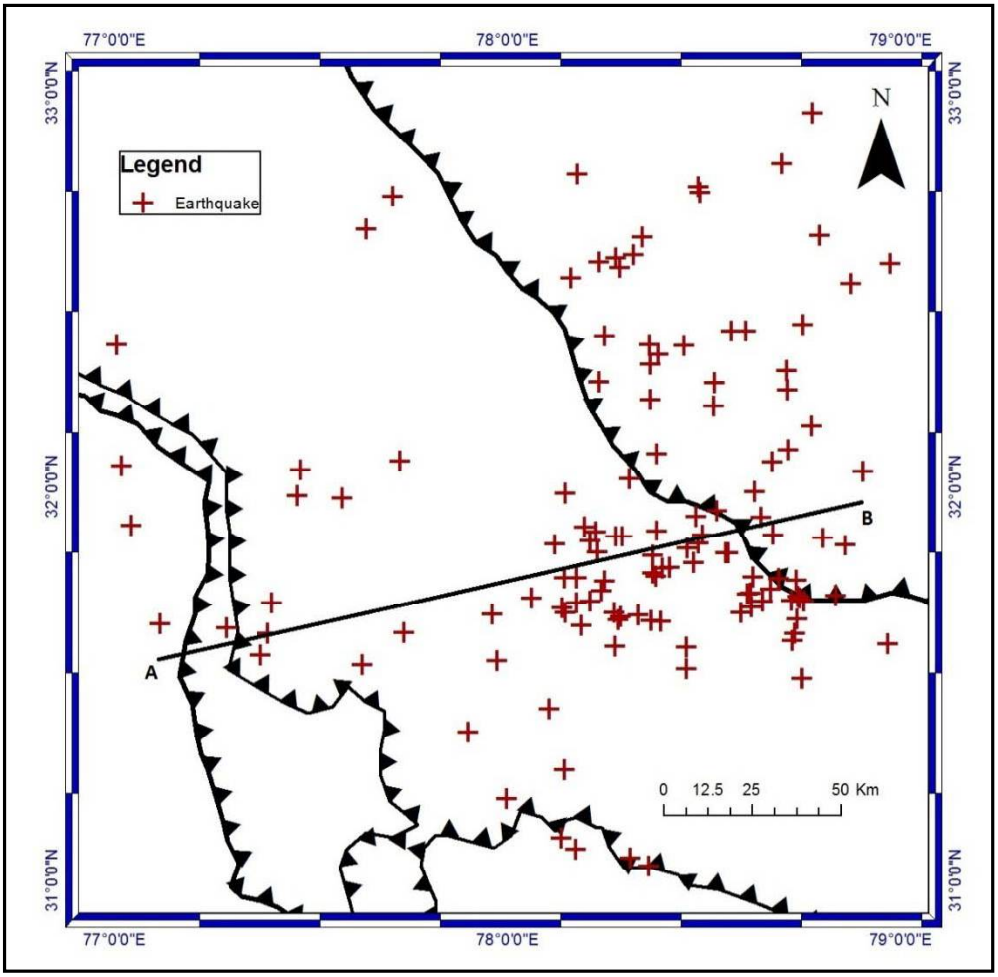

Figure 6.1: shows the transect AB (solid black line) taken across in the WWS-EEN direction cutting through major thrusts staring from MBT (Main

Boundary Thrust) in north to STD (South Tibetan detachment) in South. The major thrust faults through which the transect pass are termed as MBT, MCT, STD from south to north. The earthquake epicentres are indicated by solid Red Cross symbol.

Due to this, it was cut across the major faults in the region starting from MBT to STD shown in Figure 6.1. Figure 6.2 completely summarizing the depth distribution of events along various thrusts cut through the transect AB. There are also some new faults and lineaments along with the major thrust faults of MBT, MCT, STD and ITSZ to account for the increased seismic activity in this region in recent years. So, the optimal 1 D Velocity model calculated here is highly efficient to be used as an input model for local 3D tomography in future.

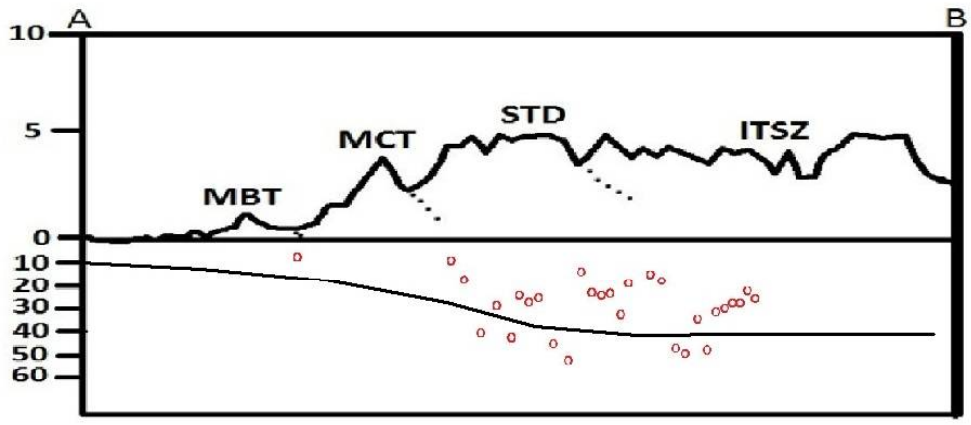

Figure 6.2: shows the focal depth distribution of seismic events (hollow red circles) across major tectonic boundaries. Such as MBT: Main Boundary Thrust; MCT: Main Central Thrust; STD: South Tibetan Detachment; ITSZ: Indus-Tsangpo Suture Zone; from south to north.

6.3. Microseismicity, Tectonics and seismic potential of NW Himalaya

Seismicity in the Himalayan arc varies greatly with space and time. This variation may result due to different causes, for example due to variation in the plate motion or convergence rate, lithology or due to presence of

complex structures. As this part has experienced four earthquake of Mw≥ 6.0 in the past, so it can be regarded as one of the most vulnerable sites for the future earthquakes. In the present study an attempt has been made to figure out some of the unanswered questions associated with the complex NW Himalayan tectonics and its earthquake scenarios. The current analysis is carried out using the high quality seismic data that was acquired over quite a long period duration using the broad band seismometers. 423 earthquakes studied and are relocated using the hypoDD software (Waldhauser and Ellsworth, 2000). A newly estimated local 1 D crustal velocity model is also utilized for the seismicity relocation analysis. The seismic events that are utilized for the study are having an uncertainty ≤ 2 km for all location parameters. The seismicity relocation has greatly helped in the current assessment of seismicity in the study region. The Main Himalayan Thrust (MHT) over which Himalaya is placed has been continuously deforming in the southward direction through different splays, viz. MCT, MBT and HFT with its northward movement. The geometry of the MHT plane have been deduced in this study which varies along the strike of the Himalaya in flat and ramp segments and its dip varies from 4° to 19° below the HFT in south to STD in the north. The depth of the two reported crustal ramp in the region the mid-crustal ramp and great Himalayan ramp below the MCT and STD varies from 12 to 22 km and 28 to 40 km depth, respectively. The earthquakes associated with all the tectonic subdivisions of the area are having focus distribution depth of 2 to 47 km that infers upper as well as lower crust deformation. The earthquake focus exhibits a bimodal depth distribution characterizing the seismogenic nature of the entire Indian crust. Again to have greater insights into the fault kinematics of the area the moment tensor solutions were estimated for eight $M_w \geq 4.0$ earthquakes which occurred in the area. The strike of the most of the solution is NNE–SSW directed that is perpendicular to the strike of the Himalaya. The observed seismicity in the region signifies a higher level of tectonic activity in this region. In another attempt an approach is undertaken to estimate the future earthquake magnitude potential prevailing

in the western Himalaya seismic gap that lies between the epicentral zone of the 1905 Kangra earthquake and the 1975 Kinnaur earthquake.

As per the calculation based on this relation $Mw=2/3\log_{10}M_0-10.7$ (Kanamori, 1983) by considering the present rates for convergence and seismic energy release in various small and large earthquakes (ISC-EHB catalogue; WIHG catalogue) only a fraction (3–5%) has been released of the total accommodated (95–98%,).

where, M_0 in the above equation is $\mu\times slip\times length\times width$,$\mu$-Modulus of rigidity is $3.3\times1011 dyne/cm^2$, and final M_0 is $10^{(1.5\times (Mw+10.7)}$.

The perpetual northward under thrusting of the Indian plate since the Late Cretaceous (Gansser, 1964, Avouac and Tapponnier, 1993; Harrison et al, 1992, Molnar and Tapponnier, 1975) under the Eurasian plate is a prime energy source for earthquakes related with MHT and its splays (Seeber et al., 1981). The rates calculated with the help of long geological (Powers et al., 1998) and short geodetic rates (Banerjee and Burgmann, 2002; Jade et al., 2011) suggest 14±2 mm/yr and 14±1 mm/yr convergence, respectively in the Himalaya. The Himalayan surface has been ruptured by several great earthquakes since the last century (1905 Kangra Mw 7.8; 1934 Bihar-Nepal Mw 8.1; 1950 Assam Mw 8.4; 2005 Kashmir Mw 7.6, 2015 Nepal Mw 7.8) (Kumar et al., 2010, Sapkota et al., 2013; Galetzka et al., 2015) and a portion of the total accommodated energy has been released during these events. The various major seismic gaps in the Himalaya (western gap, central gap and eastern gap) (Srivastava et al., 2015) have still been left to release the accommodated energy in the form of elastic deformation (Bilham et al., 2001). The present study is focused on the western seismic gap specifically in between Kangra 1905 (Ambraseys and Bilham, 2000, Kumar et al., 2010) earthquake and 1975 Kinnaur earthquake (Khatri et al., 1978). A calculation for the amount of accommodated and release energy has been conducted for this gap. As per the calculation based on this relation $Mw=2/3\log_{10}M_0-10.7$ (Kanamori, 1983) by considering the present rates for convergence and seismic energy release in various small and large earthquakes (ISC-EHB catalogue; WIHG catalogue) only a fraction (1-2%) is being released of the total accommodating (*Table 6.2*). By considering the present status, it may be

inferred that the total amount of energy released since the last great event is only a fraction of the accommodated energy and is not sufficient to prevent a giant upcoming event.

Western Himalaya seismic gap that is about 200×100 km in area is accommodating the strain in flat and ramp geometry of the MHT plain. In this geometry three different scenarios have been attempted to calculate the earthquake magnitude potential. Himalayan front has been ruptured often with giant events (Mw>8.0) as reported earlier by various researchers (Wesnousky et al., 1999, Lave et al., 2005, Kumar et al., 2006, Sapkota et al., 2013) with an average slip rate in the order of total shortening rate across the range as per GPS measurements (Avouac, 2003).

Sub-surface geometry consisting of flat and ramp of the MHT plain is well documented and it varies along the strike of the Himalaya (Caldwell et al., 2013). The NW Himalaya comprising Garhwal and Himachal section is also characterized by flat and ramp geometry consisting of two crustal ramps below the MCT in Higher Himalaya and the STD in the Tethys Himalaya. This phenomenon observed in the region can act as an individual entity with a capability to trigger great earthquakes. Hence, from this study, three different scenarios associated with the great earthquakes rupture and the ramp-flat geometry of the MHT for the NW Himalaya is proposed.

By considering the present status it may be inferred that the total amount of energy released since the last great event is only a fraction of the accommodated energy and is not sufficient to prevent a giant event in future. Three different scenarios can be proposed from the present study for having a deeper insight into earthquake scenarios of this segment of the NW Himalaya. As mentioned above these three different scenarios can be explained as follows:

Scenario I: If the flat of the MHT is 70 km wide and is participating in strain accumulation since the last event then it has approximately accommodated seismic moment M_0 7.1 E+27 dyne-cm which is equivalent magnitude to moment magnitude Mw 7.9.

Scenario II: If the mid crustal ramp below the higher Himalaya that is about 35 km wide has accommodated about M0 3.6 E+27 dyne-cm and would

result in Mw 7.6.

Scenario III: If the flat and ramp together participate in a single giant earthquake like last century 1934 and 1950 earthquakes and that would be result in a ≥8.0 Mw event.

This study is helpful in addressing some of the sensible questions associated with the Himalayan orogeny. The present work has utilized more number of data sets and new data sets recorded using the local seismic network that has prominently helped in improving the interpretation. These observations are important to minimize the seismic Hazard in the NW Himalayan region.

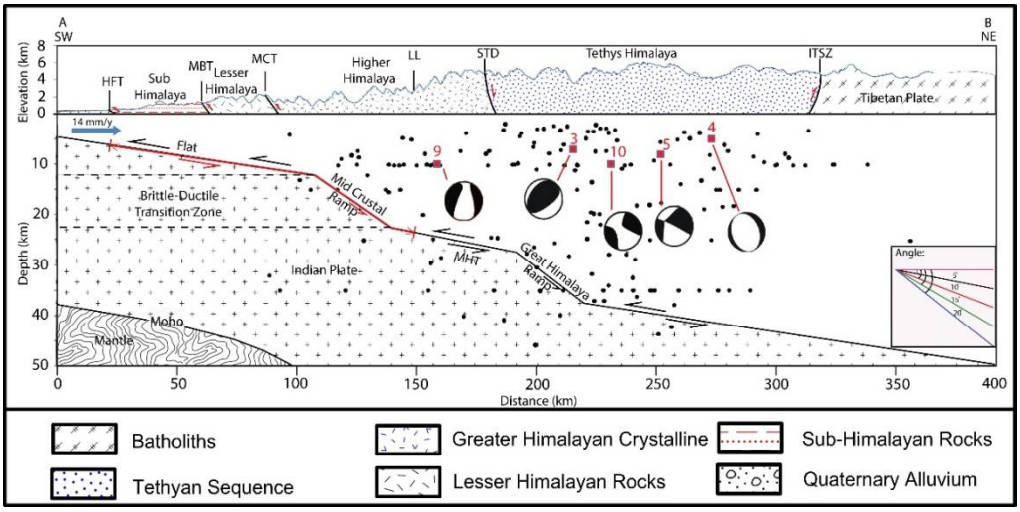

Figure 6.3: It shows the generalised cross section AB taken across the major tectonic breaks starting from the Himalayan Frontal Thrust (HFT) in the south to Indo-Tsangpo Suture Zone (ITSZ) in the north. This cross section greatly characterizes the status of the Main Himalayan Thrust (MHT) and its sub-surface geometry in the NW Himalaya. The maximum depth of the investigation below the cross section is 50 km. The cross section clearly postulates the locking zone and also the motion velocity of 14 mm/y for the Indian plate in the north direction. The section also shows the two ramps of the MHT plane below the Main Central Thrust (MCT) and the South Tibetan Detachment (STD). The depth range for these ramps is mentioned in the text.

ISC Data*					
Long	**Lat**	**Distance, m**	**Depth, km**	**Mb**	**Seismic Moment, dyne-cm**
76.63369	30.66393	0.0			
78.807	31.895	247840.4	35	5.1	5.01E+23
78	32.578	249132.7	35	5.2	7.08E+23
79.555	32.681	356065.6	25.1	5.2	7.08E+23
78.516	32.483	269715.4	18.8	5	3.55E+23
78.644	32.369	268876.4	13.3	5.1	5.01E+23
78.49	32.368	258650.7	5	6.2	2.24E+25
78.552	31.895	228031	35	5.8	5.62E+24
78.654	32.071	247592.8	35	4.9	2.51E+23
78.577	32.485	273734.9	10.8	4.7	1.26E+23
78.563	31.878	227755.2	35	4.6	8.91E+22
78.606	32.28	259444.2	35	4.9	2.51E+23
78.596	32.498	276007.1	35	4.8	1.78E+23
78.609	31.94	235333.9	35	4.8	1.78E+23
78.53	32.535	274912.5	15	5.1	5.01E+23
78.805	32.202	267811	35	4.9	2.51E+23
78.568	32.32	259961.9	13.9	4.6	8.91E+22
78.633	32.521	280244.3	35	4.9	2.51E+23
78.581	32.518	276692.2	15	4.9	2.51E+23
78.631	31.935	236676.3	10.1	5.1	5.01E+23
78.466	32.547	272009.4	8.1	5.5	2E+24
78.72	32.015	248715.2	35	5	3.55E+23
78.702	32.038	248898.2	9.2	5.3	1E+24
78.381	31.832	210911.2	35	4.9	2.51E+23
78.706	31.904	240462.1	35	4.7	1.26E+23
78.449	31.78	212652.3	2.5	5.4	1.41E+24
78.612	32.643	289016	35	5.1	5.01E+23
78.673	32.632	291880	15	4.5	6.31E+22
78.413	31.804	211454.2	6	5.2	7.08E+23
78.467	31.821	216690.5	10	5	3.55E+23
77.268	31.442	105558.2	15	4.7	1.26E+23
76.954	31.865	137017.6	15	4.6	8.91E+22
78.014	31.045	138445	15.5	5.6	2.82E+24
78.543	32.639	284485.5	15	4.8	1.78E+23
78.049	31.089	143141.5	15	4.7	1.26E+23
77.414	31.472	116638.9	15	4.9	2.51E+23
76.673	32.303	182346.1	35	4.6	8.91E+22
78.778	30.725	205199	10	6.4	4.47E+25
78.711	30.736	198829.1	26.4	4.8	1.78E+23
78.383	31.913	216667.7	15	4.2	2.24E+22

78.245	30.752	154399.8	35	4.2	2.24E+22
76.818	31.441	88197.01	32.1	4.3	3.16E+22
77.759	31.146	120033.7	35	4.3	3.16E+22
77.272	31.291	92573.01	35	4.3	3.16E+22
78.284	31.563	186267.1	41	4.2	2.24E+22
78.417	31.985	224269.8	37	4.8	1.78E+23
78.423	32.035	228342.1	37	4.6	8.91E+22
78.14	31.124	152603.9	20	4.1	1.58E+22
78.403	32.599	272752.1	25	4.3	3.16E+22
78.122	31.667	180305.8	7.2	4.2	2.24E+22
78.51	30.874	180832.1	24.5	4.2	2.24E+22
76.727	32.368	189744	10	3.7	3.98E+21
76.65	32.784	235812.9	10.8	4.3	3.16E+22
77.426	32.872	256766.9	25	3.9	7.94E+21
78.25	31.855	202891.8	3	3.9	7.94E+21
76.978	31.525	101232.5	13.1	4	1.12E+22
78.539	32.104	241623.2	36.2	4	1.12E+22
77.709	31.352	127926.8	25.2	3.9	7.94E+21
78.254	30.866	156480.1	24.8	5	3.55E+23

Note:*

Total amount of energy released from ISC EQ data= 1.4E+26 dyne-cm

Equivalent moment magnitude= 6.7 in 45 years

Average energy release/year= 3.0E+24 dyne-cm

Average equivalent moment magnitude= 5.6

WIHG Data#					
Long	**Lat**	**Distance, m**	**Depth, km**	**Mb**	**Seismic Moment, dyne-cm**
78.281	32.554	261799.1	3.5	1.6	2.82E+18
78.697	31.9	239509.6	10	2.8	1.78E+20
78.346	32.016	221524.3	3.4	2.2	2.24E+19
76.715	31.794	125931.5	8.5	2.3	3.16E+19
78.264	31.796	199738.5	11	1.9	7.94E+18
78.365	31.939	217216.9	10.1	1.7	3.98E+18
77.939	31.322	144383.4	10	2.2	2.24E+19
77.14	31.635	118273.3	8.9	2.2	2.24E+19
77.949	31.369	147883.1	5	1.8	5.62E+18
78.485	32.745	290276.5	8.4	1.8	5.62E+18
78.485	32.764	291953.5	3.9	2	1.12E+19
78.289	31.875	207141.2	25.6	3	3.55E+20

77.505	31.66	138387.3	10	2	1.12E+19
77.957	31.549	159912.4	28.5	1.7	3.98E+18
78.637	31.995	241123.7	28.8	2.3	3.16E+19
78.786	32.636	299387.1	10.1	1.6	2.82E+18
78.236	31.852	201668.5	35.2	1.5	2E+18
78.145	31.282	159681.5	10.1	2.8	1.78E+20
78.171	31.703	186424.7	3.1	2.8	1.78E+20
78.175	32.793	278090.6	6.2	3.1	5.01E+20
77.564	31.642	140270.7	10.1	4	1.12E+22
77.408	31.569	124780.3	10	2.3	3.16E+19
77.962	31.448	153700	10	4.9	2.51E+23
78.007	31.317	149740.3	10.1	2.8	1.78E+20
78.187	31.643	183624.1	24.7	2.8	1.78E+20
78.176	31.115	155526.2	10.1	3.2	7.08E+20
78.379	31.773	206822.7	2.3	2.6	8.91E+19
76.739	31.528	96629.44	4	4.3	3.16E+22
78.198	31.085	156506.3	10	3.3	1E+21
78.34	31.034	168052.3	7.3	3.2	7.08E+20
77.715	31.712	155481.3	29.7	2.5	6.31E+19
78.406	31.792	210130.7	3.3	2.7	1.26E+20
78.602	32.396	268198.1	3.8	2.5	6.31E+19
78.967	32.559	305395.6	8.8	2.7	1.26E+20
77.284	31.64	124971.3	7.2	3.2	7.08E+20
77.386	31.63	129129.3	12.1	2.6	8.91E+19
78.866	32.509	294687.8	9.5	2.6	8.91E+19
78.71	32.246	264137.7	4.9	2.5	6.31E+19
78.583	31.749	221250.3	24.9	5.7	3.98E+24
78.632	31.77	226414.2	21.9	2.1	1.58E+19
78.254	31.814	200262.3	30.4	2.4	4.47E+19
78.253	32.406	247196.1	18.1	3.3	1E+21
78.451	32.371	256393.7	42.2	2.3	3.16E+19
78.816	31.872	247175.5	25	2.8	1.78E+20
78.723	31.63	226050.1	19.8	3.9	7.94E+21
78.736	31.662	228815	2.7	2.2	2.24E+19
78.729	31.761	233696.5	5.2	1.8	5.62E+18
78.596	31.732	221281.2	21.4	2.9	2.51E+20
78.629	31.731	223877.9	19.9	2.6	8.91E+19
78.619	31.729	222955.6	19.5	2.3	3.16E+19
78.388	31.657	200195.9	2.9	2.3	3.16E+19
78.39	31.632	198853.9	5.6	2.8	1.78E+20
78.785	32.166	263830.7	21.9	2.4	4.47E+19
77.962	31.676	169266.8	40.1	2.5	6.31E+19
78.367	32.235	239961.4	32.6	2.6	8.91E+19

78.396	31.795	209567	40	2	1.12E+19
78.363	31.659	198338.4	6.4	2.8	1.78E+20
78.242	31.76	195621.1	27.7	2.2	2.24E+19
78.753	31.707	232643.7	3.1	2.3	3.16E+19
78.399	32.063	228739.2	7.3	1.9	7.94E+18
77.896	31.378	144169.8	4.7	2.5	6.31E+19
78.647	31.707	223958.6	3.4	2.6	8.91E+19
78.142	31.987	205405	7.7	1.7	3.98E+18
78.485	31.856	220363.5	4.9	2.2	2.24E+19
78.651	31.927	237682.9	27.1	2.7	1.26E+20
78.497	31.732	213395.3	28.2	1.8	5.62E+18
78.541	31.943	230416.1	27.9	3.6	2.82E+21
78.117	31.854	193415.1	3.7	2.1	1.58E+19
78.056	31.717	178975.8	8	2.4	4.47E+19
78.477	31.926	224488.3	7.5	1.6	2.82E+18
78.718	31.709	229874	3.8	1.9	7.94E+18
78.73	31.625	226378.4	2.7	2.3	3.16E+19
78.683	31.881	237225.2	27.9	1.7	3.98E+18
78.501	31.881	223236.4	13.6	2.4	4.47E+19
78.557	31.585	209830.5	7.1	1.6	2.82E+18
77.576	31.968	170456.1	3.7	2.7	1.26E+20
78.272	31.593	187105.3	2	2.4	4.47E+19
78.331	31.719	199624.7	46	2	1.12E+19
78.471	31.732	211344.9	59.1	2.4	4.47E+19
77.373	31.57	122931.6	8.3	2.5	6.31E+19
78.521	32.572	277467.7	18.4	2.7	1.26E+20
78.76	31.508	223233.3	31.7	2.5	6.31E+19
78.724	31.607	224951	2.2	2.2	2.24E+19
77.711	31.698	154069	10	2.4	4.47E+19
78.144	32.527	251814.2	17.8	2.6	8.91E+19
78.382	32.092	229757.7	34	1.6	2.82E+18
78.283	31.669	192703.5	4.3	2.6	8.91E+19
78.302	32.769	282366.8	18.2	2.9	2.51E+20
77.414	31.475	116895.5	10.1	3.2	7.08E+20
78.281	31.662	192102.3	9.9	2.5	6.31E+19
78.363	32.372	250947.4	43.7	5.3	1E+24
79.596	31.869	311884.4	10.1	2.8	1.78E+20
79.147	31.576	259920.4	53	2.1	1.58E+19
79.522	31.749	300094.4	10	2.3	3.16E+19
79.282	32.193	303462	8	3	3.55E+20
79.64	31.66	306816.9	10.1	2.9	2.51E+20
79.369	31.59	280053.5	7.2	2.2	2.24E+19
79.481	32.09	313454.8	3.2	3.2	7.08E+20

79.123	31.562	257225.5	37.8	2.6	8.91E+19
79.138	31.485	255446.6	10	4.1	1.58E+22
78.986	31.596	246784.2	18.1	3	3.55E+20
78.123	31.703	182863.2	69.6	2.7	1.26E+20
78.221	31.476	176140.3	62.2	2.3	3.16E+19
78.27	31.557	184788	66.9	2.2	2.24E+19
78.25	31.551	182828.4	74.8	2.4	4.47E+19
78.13	31.395	164163.5	56.3	2.1	1.58E+19
78.43	31.508	195164.3	53.8	2.9	2.51E+20
77.013	32.348	190735	10	3.3	1E+21
76.859	32.598	216175.1	11.1	5.2	7.08E+23
76.968	32.547	211827.5	10.1	3.8	5.62E+21
77.197	32.205	179550.1	10.1	2.6	8.91E+19
77.062	31.992	153218.8	8	3.3	1E+21
77.06	31.895	142798	10.1	2.8	1.78E+20
78.812	32.915	324171.9	10	3	3.55E+20
78.893	33.02	337980.2	10	2.6	8.91E+19
78.881	32.856	323422.6	10	3.2	7.08E+20
78.316	32.474	256796.4	75.3	3	3.55E+20
78.382	32.35	250302.4	74.5	3.2	7.08E+20
79.512	30.975	277095.4	91.7	2.3	3.16E+19
79.567	31.027	282999.9	106.2	2.9	2.51E+20
77.642	32.661	241765.2	18.3	2.1	1.58E+19
77.704	32.734	251535.6	5.5	2.4	4.47E+19

Note:#

Total amount of energy released by Local EQ data (WIHG catalogue) = 7.2E+24 dyne-cm

Equivalent moment magnitude= 5.87 in 5 years

Average energy release/year= 1.4E+24 dyne-cm

Average equivalent moment magnitude= 5.4

Table 6.1: Earthquake energy calculation from Wadia Institute of Himalayan Geology (WIHG) Catalogue and the ISC-EHB Catalogue separately.

Case	Length, (km)	Width (km)	Assessment for per year @14mm/yr convergence		Assessment for 110 years (1905-2015)			ISC EQ Data		WIHG EQ Data		Energy released in 110 years		Remaining energy and equivalent potential magnitude	
			Seismic moment, dyne-cm	Moment magnitude	Shortening since 105 years @ 14mm/yr	Seismic moment, dyne-cm	Moment magnitude	Seismic moment, dyne-cm/yr	Moment magnitude/ yr	Seismic moment, dyne-cm/yr	Moment magnitude/ yr	Seismic moment, dyne-cm/yr	Moment magnitude/yr		
I (Flat)	200	70	**6.5E+25**	**6.5**	1.54	**7.1E+27**	**7.9**	3.0E+24	5.6	1.4E+24	**5.4**	3.33479 E+26	7.0	3.2 E+ 27	**7.6**
II (Ramp)	200	35	**3.2E+25**	**6.3**		**3.6E+27**	**7.7**							6.8 E+ 27	**7.9**
III (Combine)	200	105	**9.7E+25**	**6.6**		**1.1E+28**	**8.0**							1.0 E+ 28	**8.0**

Table 6.2: Energy estimate and its magnitude potential by considering the three different scenarios proposed from the study.

6.4. Static stress change and earthquake triggering in the NW Himalaya

The static stress change due to the four major earthquakes namely the 1905 Kangra earthquake, 1975 Kinnaur earthquake, 1991 Uttarkashi earthquake and 1999 Chamoli earthquake that occurred in NW Himalaya, India are studied utilizing the Coulomb 3.1 application. Coulomb stress change was calculated utilizing the presumed three factors.1905 Kangra earthquake shows a maximum stress associated with the MHT detachment and some of the previously shadow zone has been reactivated. For the 1975 Kinnaur earthquake we observed the reactivation of the previously seismic shadow zone. For 1991 Uttarkashi earthquake the high seismic stress was observed over the lesser and Higher Himalaya and major structural discontinuities like MBT and MCT both getting activated and triggering aftershocks. In case of 1999 Chamoli earthquake a significant stress shadow is observed in some parts of the lesser Himalaya and a significant high stress is noted on the rest part of the NW Himalaya. All the above results shows that the tectonic stress in NW Himalaya is quite high and the region is near to failure chancing major earthquakes in future.

6.5. Seismic attenuation characteristics of NW Himalaya

In this study, the QC values is estimated for the North-western Himalayan (India) region using 132 seismograms from 82 local earthquakes recorded digitally at 20 different stations and analysed them for six lapse times (10, 20, 30, 40, 50, and 60 s) and five window lengths (10, 20, 30, 40, and 50 s) at ten different frequency bands with a central frequency in the range of 1.5–28 Hz. The estimated values for a lapse time of 10 s vary from 91 to 225 at 1.5 Hz and from 1537 to 4795 for 28 Hz with coda windows ranging from 10 to 50 s. An average frequency dependent power law fit for the study region may be given as $Q_C = 116.716f^{0:9943}$. The results show that Q_C is a function of frequency in the study area; the Q_C value increases as the frequency increases. A frequency dependent relationship is also obtained for the region, which shows that there is a significant increase in Q_0 values with increasing window length, while there is a nominal decrease in the degree of frequency dependence (n). This may indicate that the scattering effect in the region

exhibits a decreasing trend with increasing depth (Aki, 1980) which may be caused by a decrease in the level of heterogeneity of the medium. The estimated *Q* values show a systematic variation with different combinations of lapse time and window length. The effect of the larger lapse times can be observed in the deeper parts of the Earth, indicating that Q_0 increases and *n* decreases with increasing depth. The general trend of the present coda attenuation study results is similar to that in seismically and tectonically active regions in other parts of the world.

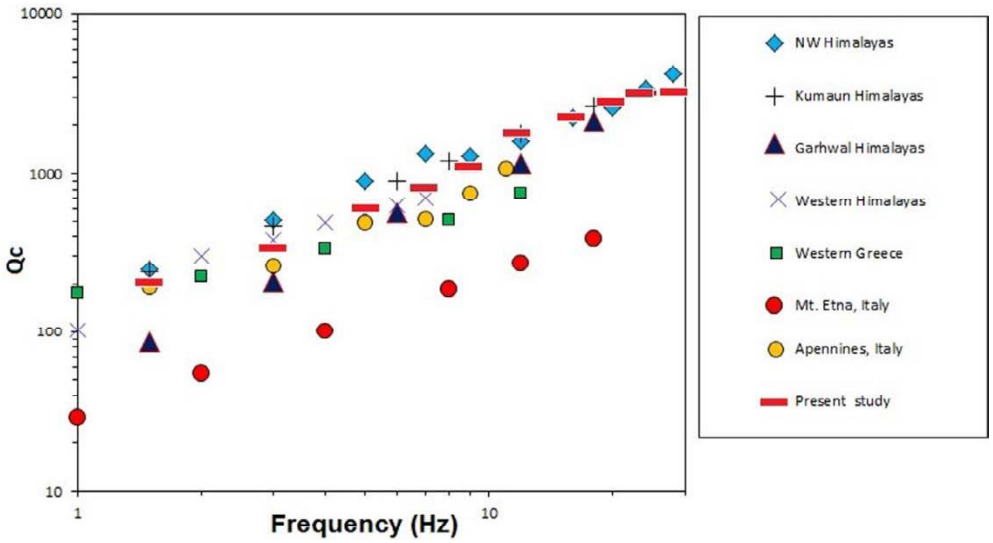

Figure 6.4: Comparison of the values obtained in this study with others estimated for various regions in the world. The regions are NW Himalayas (Tripathi et al., 2012); Kumaun Himalayas (Singh et al., 2012); Garhwal Himalayas (Gupta et al., 1995); western Himalayas (Mukhopadhyay and Tyagi, 2007); western Greece (Tselentis, 1998); Mt. Etna, Italy, (Pezzo et al., 1995); Sikkim Himalayas (Hazarika et al., 2013); Apennines, Italy (Bianco et al., 2002); and this study (LT =50; WL = 30)

6.6. Gravity anomalies and Lithospheric structure of NW Himalaya

The Bouguer gravity anomaly obtained utilizing the EGM2008 (Pavlis et al., 2008), global gravity model has been utilized to constrain the lithospheric structure of the NW Himalaya. This EGM2008 gravity model consists of the global gravity data acquired through the GRACE satellite

mission for the area where no or very less amount of terrestrial data is available. These less availability of the gravity data is mainly due to the inaccessible conditions of the difficult high terrains for e.g. Himalaya. The Bouguer anomaly data derived here are very much useful in delineating large scale geological subsurface features present in the NW Himalaya.The use of the EGM2008 gravity model gives the major advantage of more resolution over other global gravity model e.g. EIGENGL04C, it contain more terrestrial gravity data that gives a better representation to short wavelengths (Tiwari et al., 2010). The GTOPO30 (GTOPO, 1997) digital terrain model has been utilized to take care for the Terrain corrections. There is also a Bouguer slab corrections applied for a density of 2.67 g/m^3. Filtering is applied to the data at 50 km wavelength. Then after applying this filtering to the Bouguer gravity data it is represented with Figure 6.5 for the NW Himalaya, India-Eurasia collision zone. The Bouguer gravity anomaly obtained for the region suggests compensation of topography at depths accounting for a flexural structure beneath the surface.

Figure 6.5shows Bouguer gravity anomaly computed for the NW Himalaya region along with the studied profile AB. The Bouguer gravity anomalies observed delineates with significant highs and lows towards the SW and NE ends respectively for the entire studied region with a consistently lower value at higher topographic elevations. The gravity highs are observed for the Indo-Gangetic Plain (IGP), Siwalik Himalaya (SH) and the Lesser Himalaya (LH) and significant lows are observed over Higher Himalaya and mostly in the collision zone of Tethys Himalaya. However, gravity anomalies also reflect low and high-density crustal rocks, which, however, can be delineated only after the effect of the crustal thickening and thinning is separated out as the regional field from the observed field that presently dominates the observed field. Therefore, the gravity anomalies are analysed using suitable wavelength filter based on coherence analyses of Bouguer anomaly and topography.

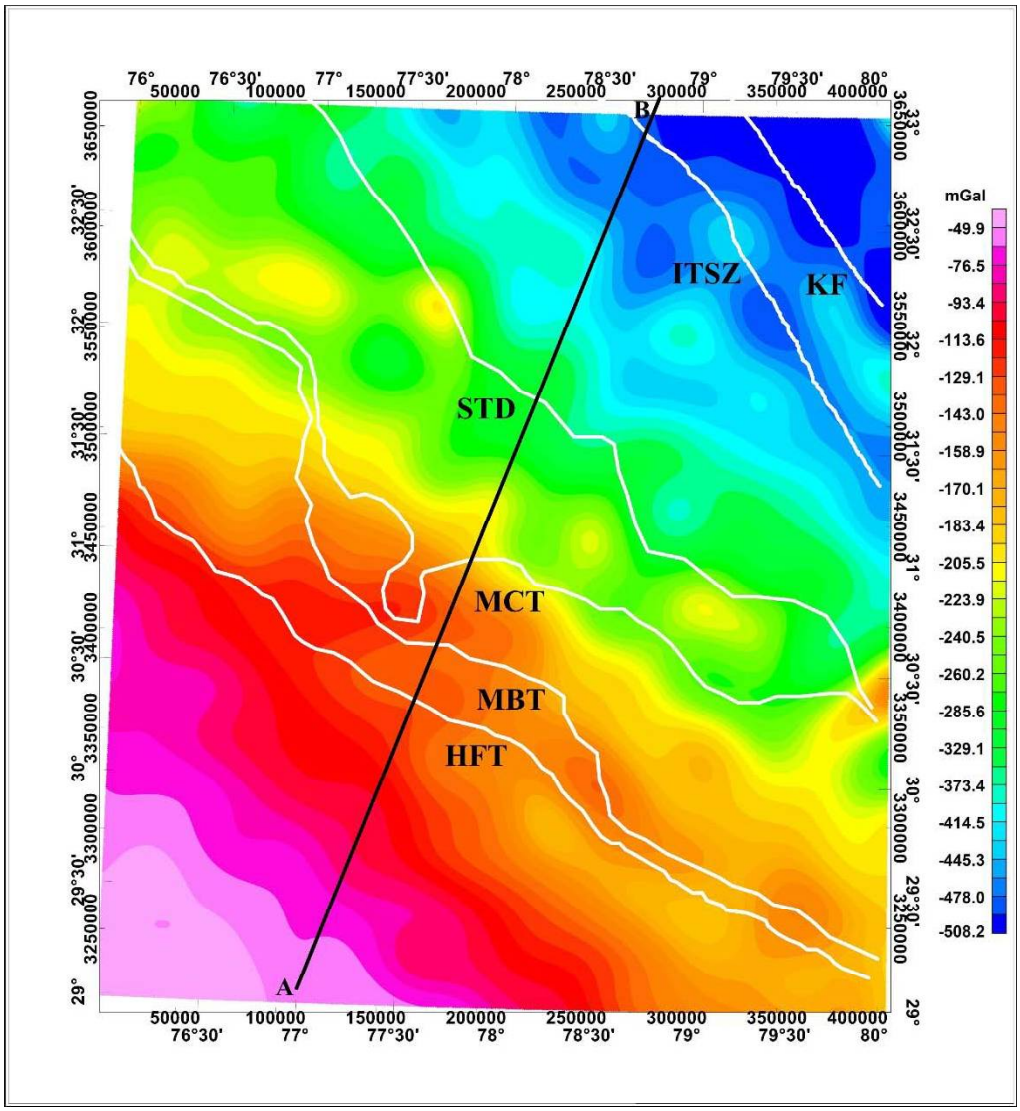

Figure 6.5 shows Bouguer gravity anomaliesof the NW Himalaya. Major tectonic boundaries in NW Himalaya along with the studied NE-SW profile. ITSZ: Indus-Tsangpo Suture Zone; MCT: Main Central Thrust; MBT: Main Boundary Thrust; HFT: Himalayan Frontal Thrust; STD: South-Tibetan Detachment. A SW-NE profile (A-B) is shown along which a lithospheric density model is shown in Figure 6.8.

6.6.1. Isostatic studies and Effective elastic Thickness (EET)

The higher elevated topography are very well compensated with varied mechanism of Isostatic compensation. This phenomenon is being widely supported with isostatic compensation of continental topography which further

implies that subsurface loads are reinforced by the strength of the lithosphere (Tiwari et al., 2010). Thiseffective strength of the lithosphere and its intrinsic property can be determined using the Effective Elastic Thickness (EET) as a proxy (Tiwari et al., 2009). The EET is defined as the response of the lithosphere due to the topographic or geological load over a time (Watts 2001and reference therein). This implies that in this part of the lithosphere, strain is proportional to the stress and beyond certain limit of stress; the rocks fail to produce seismic activity. EET estimated for continental regions has been of great importance (McKenzie and Fairhead 1997) in the recent times. EET is estimated by different approaches (Watts 2001). The most popular approach to estimate EET is based on coherence between Bouguer anomaly and topography accounting both surface and subsurface loads (Forsyth 1985). In the present study, a similar approach of computing coherence between the Bouguer gravity anomaly and topography encompassing the whole NW Himalaya using the MEM method (Lowry and Smith 1994) are utilised. Estimate of EET from coherence analysis is based on the assumption that long wavelength topography is isostatically compensated and, therefore, topography and the Bouguer gravity anomaly are coherent; whereas at short wavelengths, topography is uncompensated and, thus, Bouguer gravity anomaly is incoherent with topography (Forsyth 1985). The roll off, on which coherence increases, is marked as the wavelength of isostatic compensation. Figure 6.6 shows an estimated EET as 53 km along with observed and best fitted coherence curve. Again in order to have a better constraint on the estimated EET for the NW Himalaya, the error in the coherence analysis utilizing the wavelet approach designated by Swain & Kirby (2003) has been applied. The resulted error in residual is plotted as a function of Effective Elastic Thickness (Te) shows a minimum error and maximum coherence at 53 km. Therefore 53 km is taken as the computed Effective Elastic Thickness (Te) for the NW Himalaya region. Figure 6.7 describes the accounted error in residual for different Effective Elastic Thickness (Te) for the NW Himalaya, India-Eurasia collision zone.

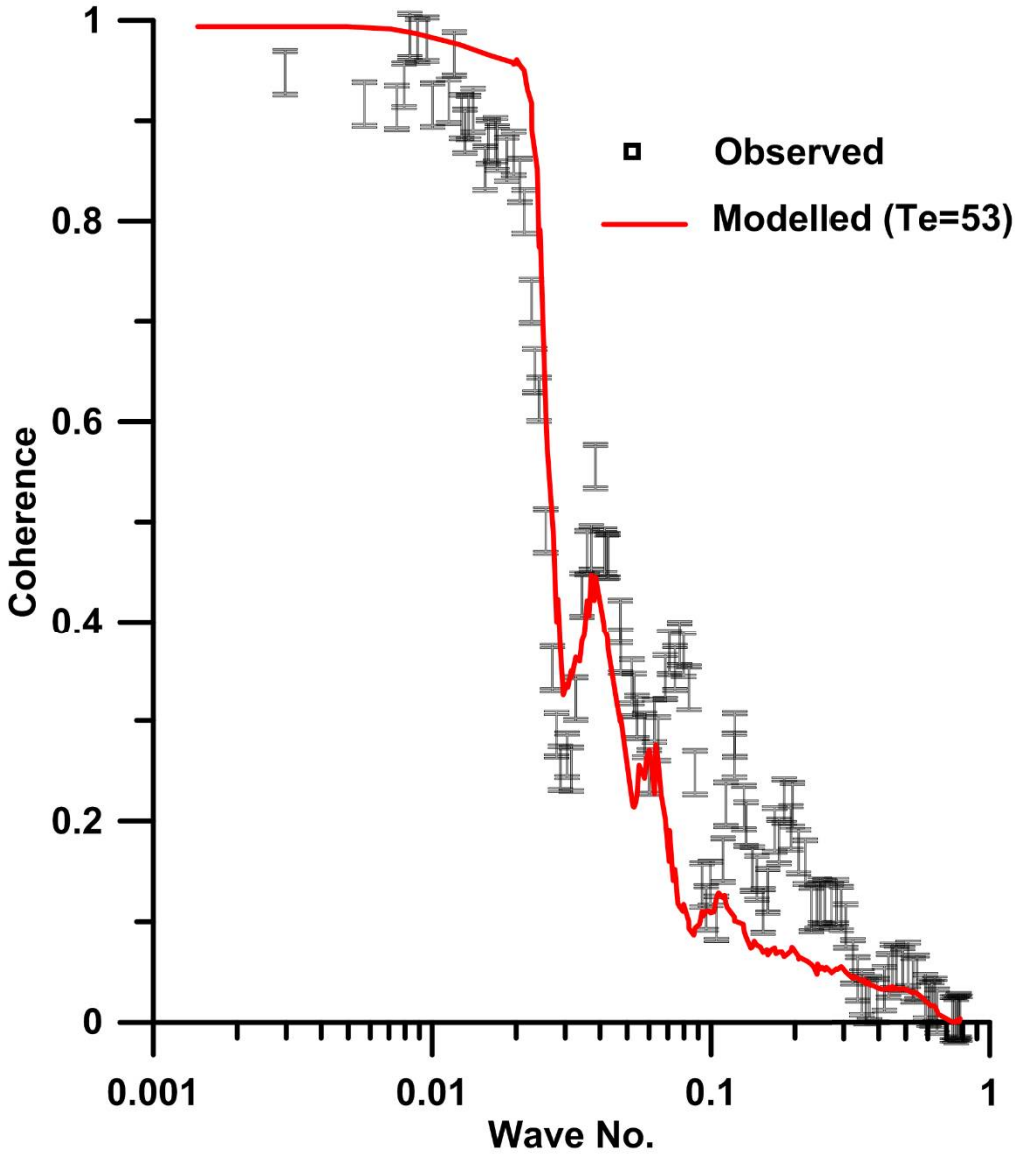

Figure 6.6: Effective Elastic Thickness (Te) based on coherence between the Bouguer anomaly and topography. The best fit is obtained for Te=53 km.

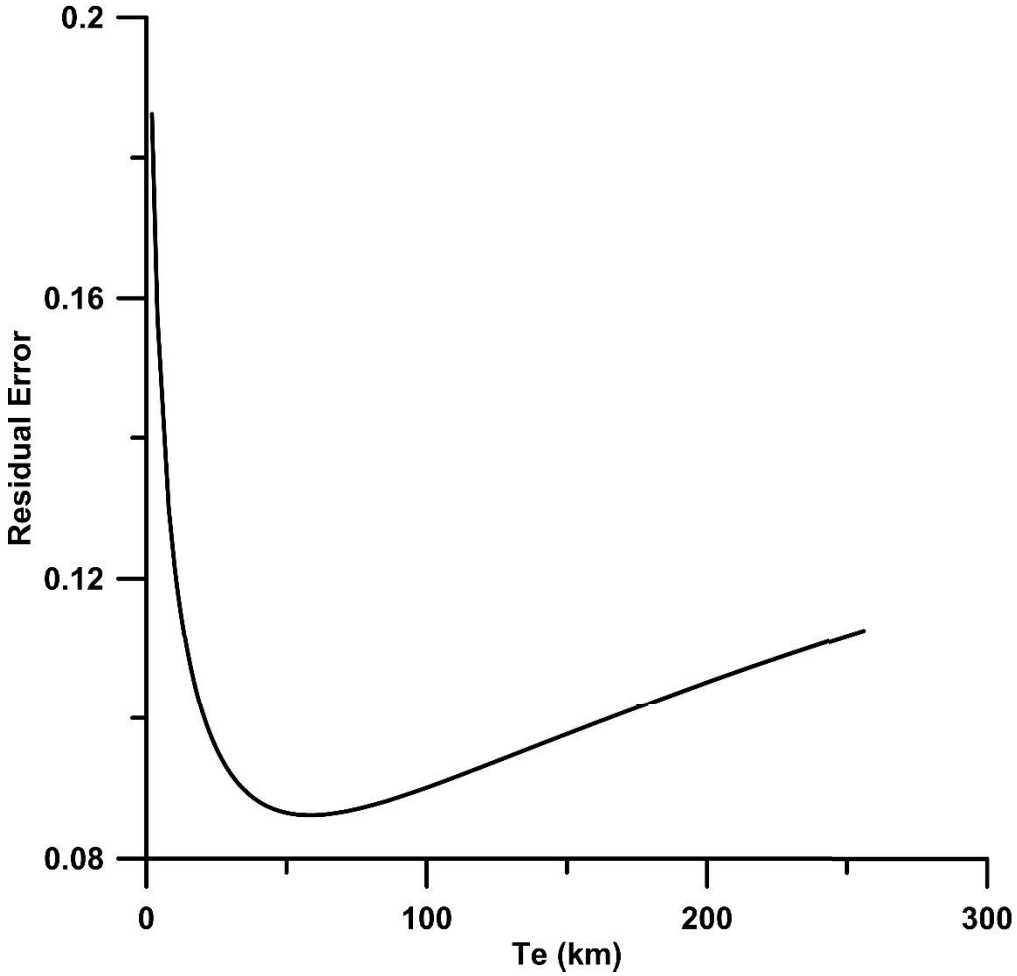

Figure 6.7: Accounted error in residual for different Effective*Elastic Thickness (Te) with a minimum observed at 53 km for the NW Himalaya, India-Eurasia collision zone.*

6.6.2. 2 D Density model for NW Himalaya

A 2D density modelfor the NW Himalaya has been constructed utilizing the Oasis montaj gravity modelling software (Tom et al., 2009). This modelling is done based on the forward modeling of the gravity responses of the modelled bodies of different geometries and are compared to the observed Bouguer gravity anomalies. This type of density modelling depends on the geometries of the subsurface bodies. Here the 2 D density modelling is carried out alongthe SW–NE profile to understand the seismotectonics of the region. The initial constraint to the model is based on the model obtained with the seismological studies earlier in the region shown in figure 6.3. The shape and

size of the modelled bodies are modified in order to obtain a best fit between the observed and calculated Bouguer gravity anomalies. The SW–NE vertical cross-section shown in figure 6.8 designates the modelled lithospheric structure beneath the studied profile. The model shows that the gravity high originated from the high density thrusted rocks along the major thrust boundary. The gravity low is coinciding with region of deep rooted Moho in higher Himalayan region.

The model shows Moho depth of about 35–37 km in the Indo Gangetic plain (IGP) towards the south of the HFT and it gradually extends to about 40-45 km beneath MBT and about 50 km below the MCT. The Moho depth gradually increases and reached about 55–60 km beneath the STD and it reaches a maximum of 75–80 km below the ITSZ, which defines the boundary between the India-Eurasia plates in the NW Himalaya. This Gravity modelling along the SW–NE profile crosses the major tectonic element in the NW Himalaya is modelled as the large wavelength gravity anomalies which are interpreted due to crustal thickening. After confirming the regional structure of the region we modelled the short wavelength gravity that is interpreted due to high density thrusted rock along with ramp of Main boundary Thrust and mid crustal density heterogeneities.

The most prominent feature along the profile is found with the zone of ITSZ. Beneath the ITSZ there are high and low density short wavelength feature is found which might be emplaced during the evaluation of the ITSZ. Further we combined the tectonic interpretation of gravity model with seismicity of the region and interpreted seismotectonic of the study region. The hypocenters of earthquakes are concentrated in narrow zone of STD mostly along the Kauirik fault which is seismically very active. The earthquake are concentrated in the depth range of 5-20 km similar to the other sector of Himalayan region. Hence, from the above observations it is clear that the regions of high tectonic activities are compensated with low gravity values and high topography. This implies in the NW Himalaya that the higher tectonic provinces are characterized with shallower crustal seismicity as recorded with seismological modelling and supplemented with the gravity observations.

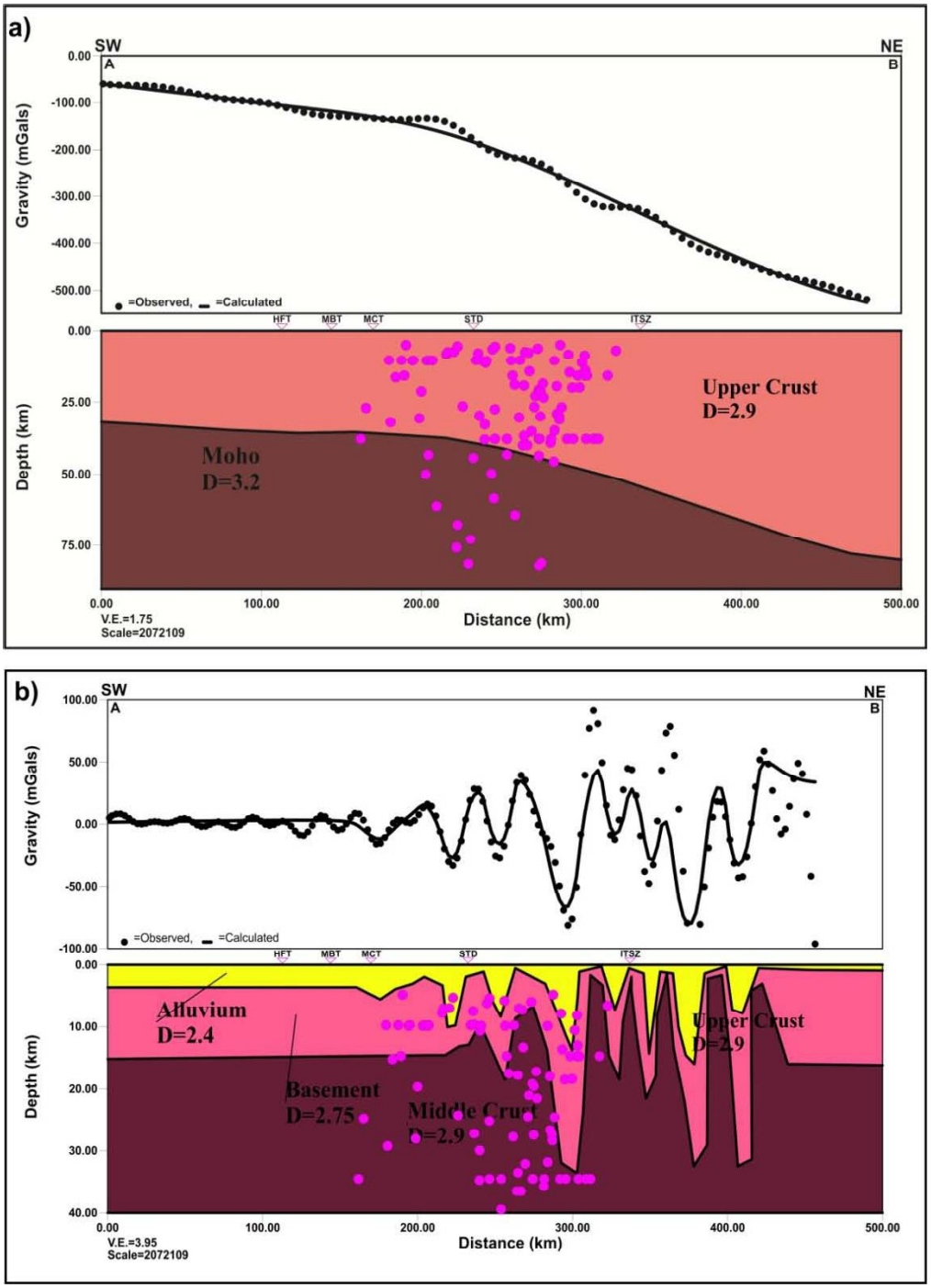

Figure 6.8: Observed and calculated response from gravity data and the corresponding lithospheric model (Bottom) for NW Himalaya – (a) Regional and (b) Residual.

Therefore the present integrated approach of the seismological and geophysical study refine the crustal structure beneath the NW Himalaya characterizes a thicker crust with entire seismogenic Indian crust.